ACS OMEGA

Open Access

http://pubs.acs.org/journal/acsodf

Article

3D Printing of Thermally Responsive Shape Memory Liquid Crystalline Epoxy Networks

Collin Pekol, Jacob Furst, Yuzhan Li, Jong Keum, and David P. Harper*

Cite This: *ACS Omega* 2024, 9, 40801−40809

Read Online

ACCESS | Metrics & More | Article Recommendations | Supporting Information

ABSTRACT: A two-component liquid crystalline epoxy network (LCEN) with shape memory behavior was developed and evaluated as a candidate material for 3D printing. The cure kinetics of the uncured material and the shape memory properties of the cured LCEN were investigated by using parallel plate rheology and dynamic mechanical analysis, respectively. A commercially available fumed silica additive was introduced to the neat, uncured material to improve the rheological properties for 3D printing. The addition of fumed silica was found to increase the yield stress, shear-thinning behavior, and toughness of the uncured epoxy ink. Polarized light microscopy, differential scanning calorimetry, and wide-angle X-ray scattering measurements between the neat and additive-modified LCEN suggested a reduction in liquid crystalline alignment in the modified LCEN, owing to interactions between crystalline domains and fumed silica, which in turn influenced the mechanical behavior. Overall, the additive was found to be successful in preserving the shape memory properties of LCEN while improving its printability.

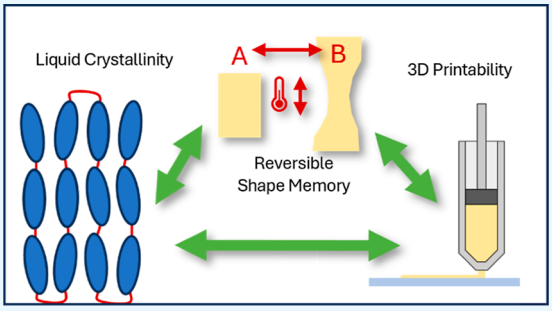

1. INTRODUCTION

3D printing has seen much recent development as a method for producing functional and structural components from thermosetting materials, such as epoxies. Applications have included aerospace components, actuators, vibration damping, insulation, and smart adhesives.[1−9] However, it must be noted that significant challenges remain in 3D printing techniques. Material candidacy, for example, is one such limitation. Relatively few materials are readily suitable for 3D-printing, especially when conventional methods of forging, casting, thermoforming, and other processes are considered. Furthermore, the predictability of materials in terms of their inherent printability under different print conditions can be difficult to discern as no comprehensive standardized method of ascertaining printability exists. In addition to materials selection concerns, 3D printing also introduces a set of unique mechanical challenges. Anisotropic tensile strength, particularly in the *z*-direction of the printed part, is an area of great concern in 3D printing technologies, where fused deposition modeling (FDM), the most common type of industrial and consumer additive manufacturing, is utilized.

Epoxy inks have shown promise as an avenue for addressing some of these concerns in 3D printing. First, the rheological properties of epoxy inks are readily tunable via commercially available additives such as fumed silica.[10,11] Such additives have been shown to introduce or augment shear thinning behavior into the ink. Shear thinning allows the high shear of the print nozzle to lower the apparent viscosity of the epoxy ink during printing and then allows the lower shear environment of the layer-by-layer deposition to appropriately accommodate an increased apparent viscosity. The increased viscosity may inhibit thermal creep and increase the bead integrity. One such epoxy ink with promise for 3D printing is the two part system of the monomer 4,4′-bis(2,3-epoxypropoxy)biphenyl and sebacic acid which react and cross-link to form a liquid crystalline epoxy network (LCEN).[12] The LCEN is a thermally responsive system that is capable of shape memory and self-healing when exposed to temperatures above its liquid crystalline (LC) isotropic transformation temperature (T_i) during which LC domains lose internal directional ordering of the mesogens in a reversible transformation. This LCEN's shape memory characteristics are of special note as it is described by reversible 2-way shape memory, contrasting the one-way shape memory mechanism of most shape memory alloys.[13] Many shape memory polymer systems facilitate shape memory through the release of internal strain in a cross-linked network by raising the temperature above a transition temperature, though other stimuli such as magnetism, pH, and light have also been demonstrated as means for triggering shape memory.[14−16] In the case of the LCEN, the individual LC domains align their orientational ordering under sufficient tensile loading along the loading direction such that the

Received: June 17, 2024
Revised: August 9, 2024
Accepted: August 14, 2024
Published: September 17, 2024

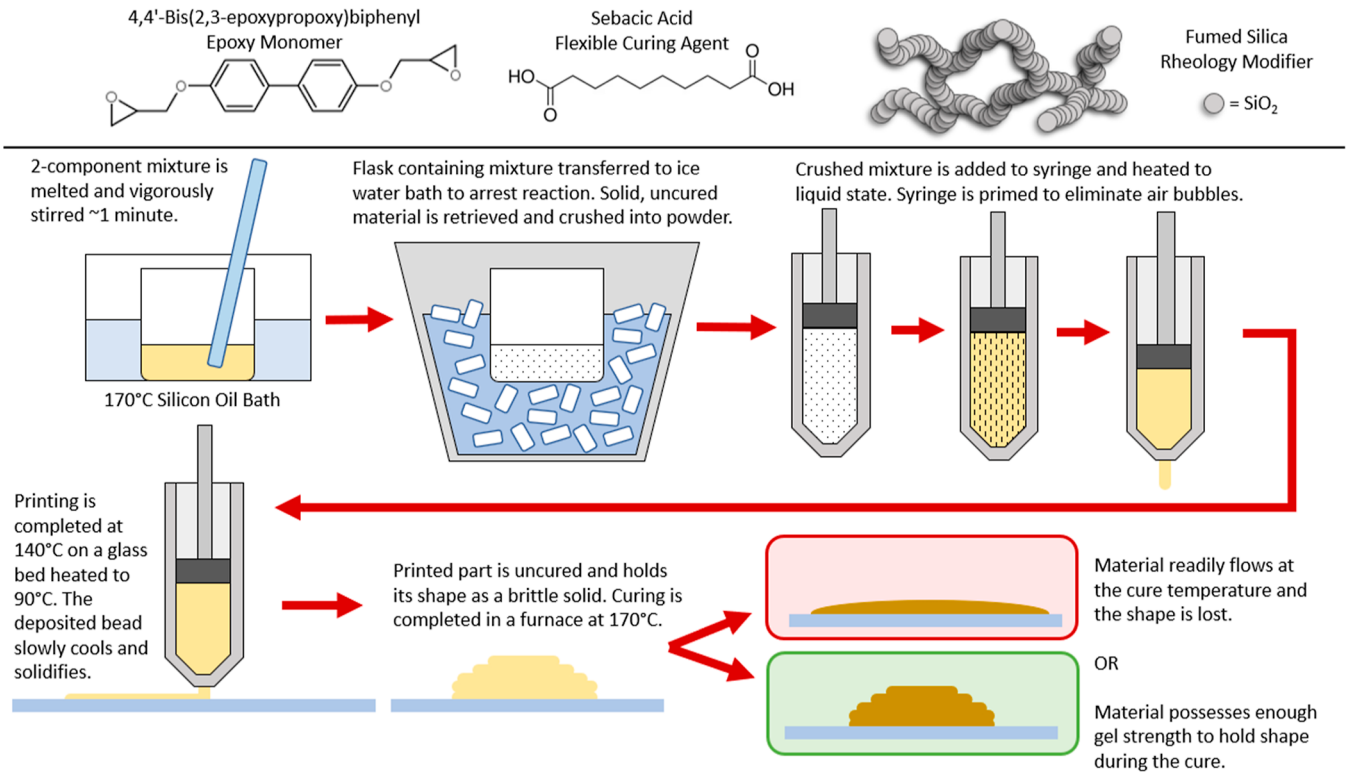

Figure 1. Methodology and chemistry of 3D printing the LCEN are outlined from mixing to syringe-loading, to extrusion, and then finally curing. It is noted that the most significant point of failure is maintaining bead integrity during cure. The final step of the process highlights the rheological need for precure LCEN to maintain its shape at high temperatures.

previously polydomain structure becomes more united in a monodomain structure in what is referred to at the polydomain−monodomain (P−M) transformation.[17] The P−M transformation is often accompanied by large magnitudes of strain, which is reversible across T_i. The system has been shown to possess favorable thermal cyclability and can be considered a candidate for many "smart material" applications such as functional coatings, actuators, soft robotics, and tunable optical systems.[18−22] The monomer is composed of rigid aromatic rings that give the monomer strong anisotropic properties. Additionally, the reactive sites of the monomer include strained epoxy rings. The reaction of the monomer with sebacic acid includes the exothermic process of epoxy ring-opening. This reaction produces no harmful byproduct and results in a latent heat cure. This allows the mixture to maintain fluidity above a melt temperature before cross-linking and rigidly curing at a higher cure temperature. Furthermore, the cure time can be further delayed near-indefinitely by keeping the uncured mixture chilled below room temperature. In this environment, the material takes on brittle, glassy behavior and can be easily crushed and powdered for later remelting.

Attempts to 3D print with the powdered material using a heated reservoir print head yielded mixed results. The mixture can be easily heated to a sufficient melting temperature and printed during the time of the latent cure with the deposited material cooling to a brittle state on the printing stage. The resulting printed part possesses the desired geometry; however, a final heat treatment is required to complete the latent cure, and this can lead to a reduction in viscosity of the uncured material, causing it to readily flow and lose its original printed shape. The general methodology for attempts to 3D print the neat LCEN are outlined in Figure 1, noting that the latent heat cure allows time for the mixed two-component system to be printed via FDM. Though neat uncured LCEN lacks the structural integrity at the cure temperature to maintain the print geometry, formulations of LCEN modified with fumed silica demonstrated sufficient structural integrity to maintain shape during the cure process.

In this work, we demonstrate a method for 3D printing LC epoxy ink with rheology-modifying additives. The purpose of the rheology modification is to improve gel strength of the uncured part such that it maintains the printed shape during the cure and preserves the functional shape memory capability of the cured LCEN.

2. METHODOLOGY

The epoxy monomer 4,4′-bis(2,3-epoxypropoxy)biphenyl was sourced from BOC Sciences. Sebacic acid was acquired from Sigma-Aldrich. CAB-O-SIL brand fumed silica was sourced from Cabot. To prepare for 3D printing, the powdered form of each component was thoroughly mixed at a 1:1 molar ratio with a glass rod in a beaker in a silicon oil bath of 170 °C. After thorough mixing for 1 min, the beaker containing the liquified mixture was transferred to an ice water bath to arrest the latent cure. The dry, uncured material was then crushed and stored in a freezer for later 3D printing. For the silica-modified system, fumed silica was introduced to the molten mixture and well stirred before quenching in an ice bath. The precured mixture was manually crushed into coarse powder via hand tools.

3D printing was accomplished using an Engine SR by Hyrel 3D equipped with a TAM reservoir printhead for heated emulsions. 15 g of uncured material with 8% fumed silica by weight was loaded into the reservoir in powdered form and

https://doi.org/10.1021/acsomega.4c05664
ACS Omega 2024, 9, 40801−40809

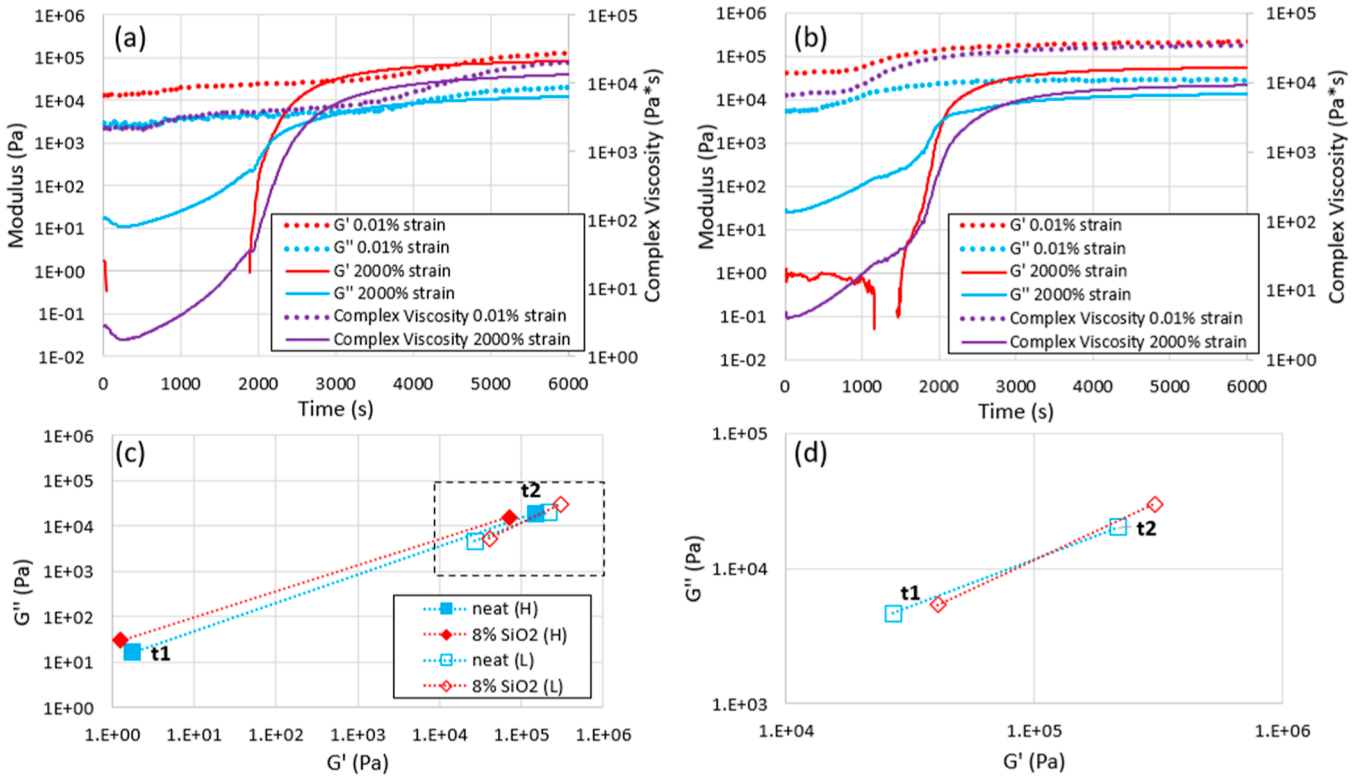

Figure 2. Oscillatory time sweeps reveal rheological evolution over time from "t_1" (0 s) to "t_2" (6000 s), shedding light on the time dependence of the latent cure system. The neat LCEN (a) and 8% wt fumed silica (b) small increases in moduli and viscosity with time as the system cures. The relationship of the precure storage and loss moduli and the postcure storage and moduli are observed to change within similar orders of magnitude for the neat LCEN and 8% wt fumed silica (c). The similarity in moduli magnitudes for both LCENs is also seen in the low-shear test (d).

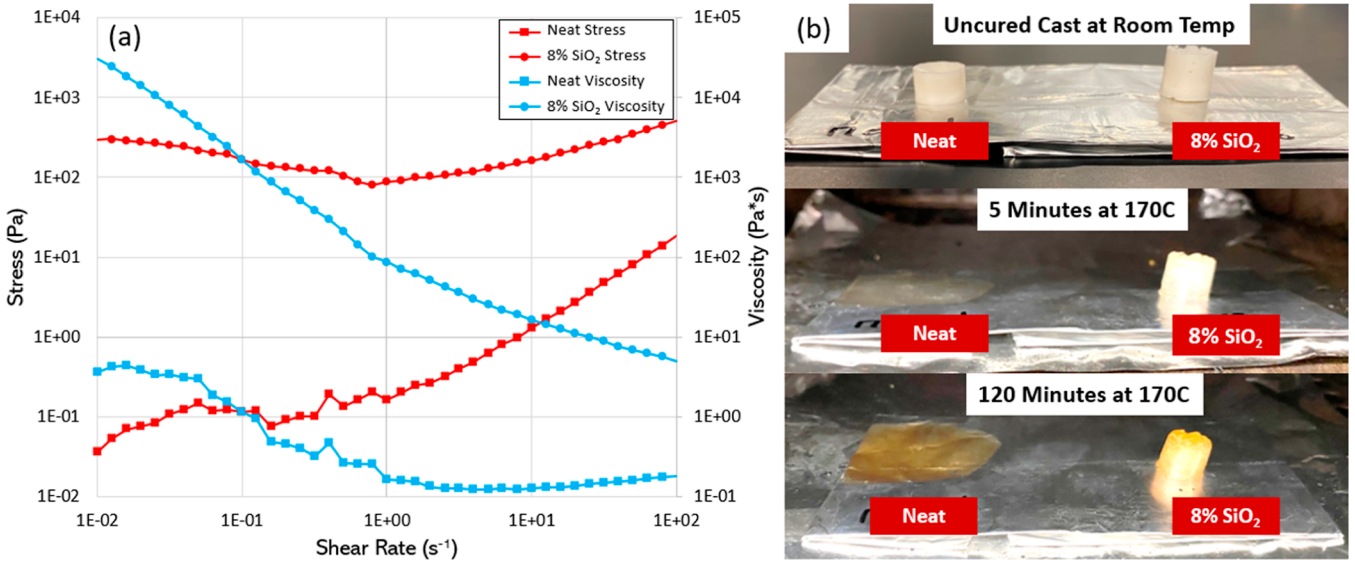

Figure 3. Nonoscillatory rheometric flow test (a) and heating of uncured 1 cm diameter pellets (b) reveal the yield stress and flow behavior of the LCEN. Yield stress of the viscoelastic fluid is determined by the average shear stress experienced before the viscosity at the same shear rate entering a regime of reduced shear rate dependence. A threshold yield strength is required for a deposited bead of uncured LCEN to maintain its shape during the latent head cure. Yield stress for the neat uncured LCEN and the modified uncured LCEN at melt temperature is found to be 0.096 and 184 Pa, respectively. The photographs on the right demonstrate how some threshold yield strength of at most ∼180 Pa is required to prevent the material from flowing past the melt temperature of the uncured LCEN.

heated to 140 °C while the print bed was heated to 90 °C. The print head was primed for 1 min to aid in the elimination of air gaps in the reservoir. The injection nozzle was primed by heating the system above the melt temperature of the mixture and manually driving the plunger until an uninterrupted bead of epoxy could be extruded. A layer of aluminum foil was smoothed over the glass print bed for removal of the printed part. After printing, the printed part was transferred to a furnace heated to 170 °C. The printed LCEN part was allowed

https://doi.org/10.1021/acsomega.4c05664
ACS Omega 2024, 9, 40801−40809

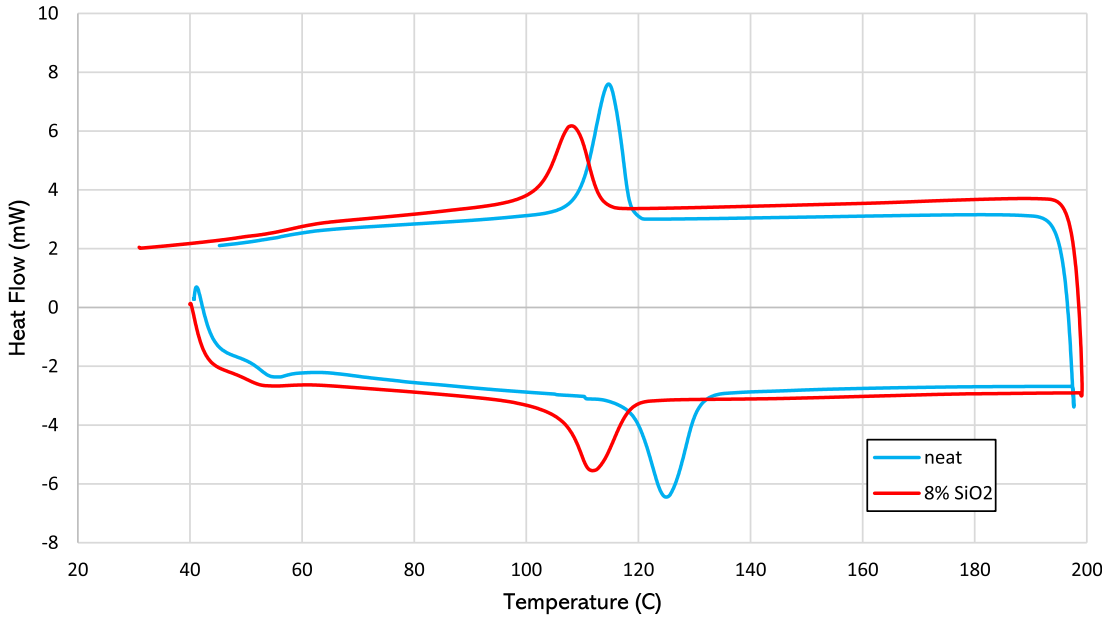

Figure 4. Representative heating and cooling cycle of differential scanning calorimetry (DSC) shows the LCEN T_i and enthalpy of transformation. The enthalpy (averaged over four cycles) was measured to be 18.46 and 15.39 J/g for the neat and modified LCEN, respectively. Calculated from additional cycles, average T_g was found to be 59.6 °C for the neat LCEN and 63.2 °C for silica modified.

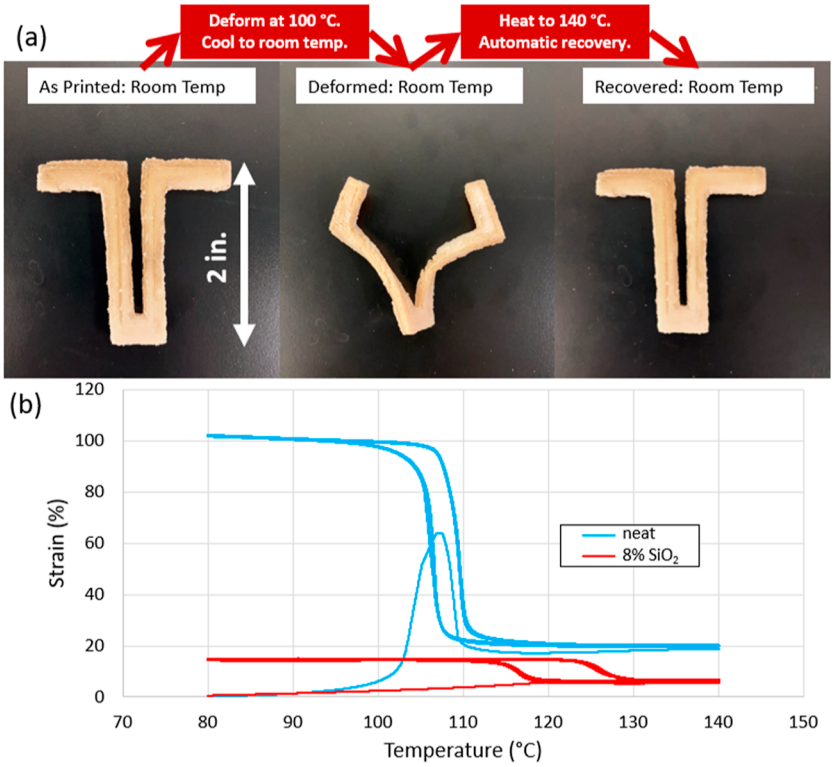

Figure 5. Shape memory of the LCEN was evaluated by deforming the fumed silica-modified print (a) and by cyclic temperature ramps between 80 and 140 °C under a constant load of 0.1 MPa (b).

to cure for at least 4 h. The completion of the cure was verified by DSC.

Cure profiles, tensile testing, and all storage and loss moduli measurements were obtained by using an ARES-G2 rotational rheometer by TA Instruments. Temperature control was provided by an enclosed forced convection oven with nitrogen gas. For viscous measurements, the rheometer was configured with 25 mm disposable aluminum parallel plates oscillating at a 1 Hz frequency. Curing was completed with this geometry as well as a layer of Kapton tape on each parallel plate such that the cured LCEN might be removed from the plates. The cured discs of LCEN were sectioned into rectangular samples ∼3 mm wide for tensile testing and shape memory tests. For tensile and shape memory measurements, tension grip fixtures for ARES-G2 were applied. In shape memory testing, the temperature was cycled across T_i while a constant load of 0.1

https://doi.org/10.1021/acsomega.4c05664
ACS Omega 2024, 9, 40801−40809

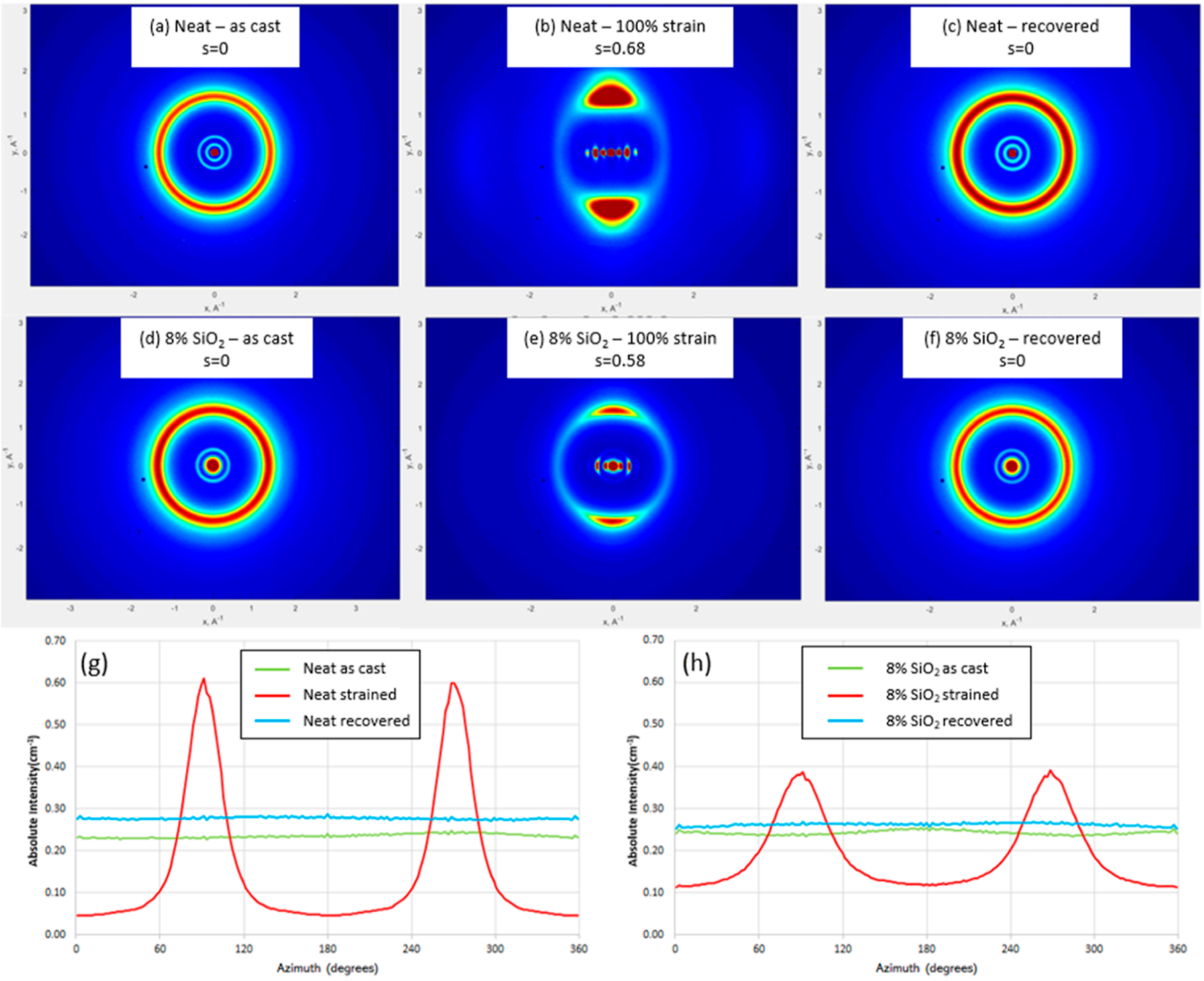

Figure 6. 2D spectra of neat LCEN in the as cast (a), strained (b), and recovered (c) states demonstrate the reversibility of the P−M transformation. Spectra for silica-modified LCEN in the as cast (d), strained (e), and recovered (f) region demonstrate a similar reversibility, but with a lower achievable orientation factor under the same strain. The azimuthal intensities for neat LCEN (g) and fumed silica-modified LCEN (h) were also evaluated with regard to the observed intensities under similar strains and with similar recovery conditions. The ability of differing LCENs to undergo the P−M transformation was quantified by calculating the Herman's orientation function (s) from the azimuthal intensity distribution of a WAXS pattern.

MPa was applied. The temperature was ramped at 1 °C/min between 80 and 140 °C such that multiple cycles under constant load could be observed. For the generation of stress−strain curves, loading was applied to the sample by increasing the gap size at a Hencky strain rate of 10%/min.

Wide-angle, medium-angle, and small-angle X-ray scattering (WAXS, MAXS, and SAXS) measurements were collected using a Xeuss 3.0 beamline instrument by Xenocs. Two 10 min exposure times were collected for each test such that the composite images free of blind spots could be constructed for each of the 2D spectra measured. Detector distances of 900, 350, and 45 mm were used for SAXS, MAXS, and WAXS, respectively. The beamline is equipped with a Geni3D detector and a Cu Kα source of 0.1542 nm wavelength.

Attenuated total reflectance Fourier transform infrared (FTIR) spectroscopy was performed with and without fumed silica addition for cured and uncured LCEN (PerkinElmer Spectrum 2). Spectra were collected from 600 to 4000 cm^{-1} at 1 cm^{-1} intervals averaged over 16 scans.

3. RESULTS AND DISCUSSION

A variety of methods can be used to describe the cure kinetics of LCEN, ranging from mechanical to thermodynamic. One mechanical method implemented is the use of parallel plate rheometry to measure the evolution of moduli and viscosity with temperature. In prior studies, the ratio of storage and loss moduli have been used as predictors for 3D printability, the rationale being that some threshold magnitude of solid-like elastic behavior from the viscoelastic printable epoxy ink is required and can be measured. These threshold values were marked by recommended minimum elastic and loss moduli and minimum ratio of loss modulus to storage modulus.[1] From Figure 2, the latent cure is seen, with a near stepwise shift in moduli and viscosity alike at the cure time near ∼2000 s. Two time-sweep techniques were evaluated: a high-shear test

https://doi.org/10.1021/acsomega.4c05664
ACS Omega 2024, 9, 40801−40809

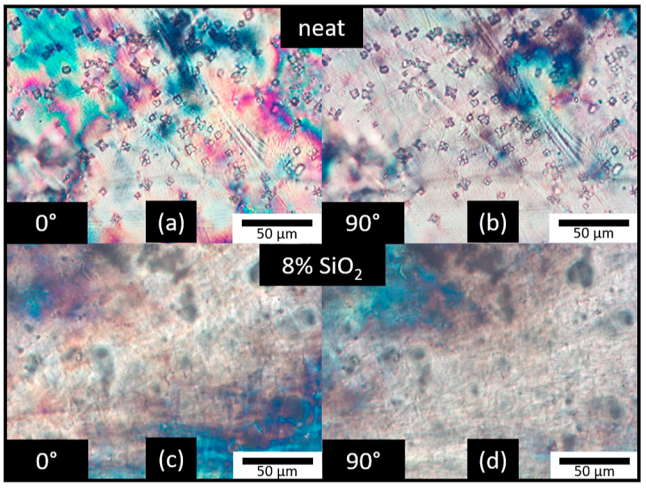

Figure 7. Neat and silica-modified LCEN is depicted under view of a set of polarizing lenses oriented at 0 and 90°. Area fractions of the visible LC domains were determined by ImageJ thresholding analysis and determined to be 42.0 and 31.4% for neat LCEN at 0 (a) and 90° (b) and 22.7 and 18.9% for modified LCEN at 0 (c) and 90° (d), respectively.

(2000% oscillatory strain) and a low-shear test (0.01% oscillatory strain) test. The aim of the high-shear test is to purposefully capture rheological measurements outside of the linear viscoelastic region of the uncured system, breaking the initial gelation and simulating the high-shear environment of the 3D printer head. The low-shear test is well within the linear viscoelastic range and best simulates the shear forces experienced by a freshly deposited bead of epoxy ink. In the low-shear test, only a relatively small magnitude increase is observed between the uncured and cured systems, suggesting that the gelation of the material is not broken in the low shear. Furthermore, the high-shear test shows a dramatic change in magnitude of viscosity and moduli from uncured to cured state, suggesting that the gelation of the uncured material had been interrupted until the energy requirement of the latent heat cure had been satisfied and the cross-linking began. Both the neat material (a) and the modified (b) show similar magnitudes and trends for their respective high-shear tests and low-shear tests, indicating that the additive does not affect the time-dependent rheological properties of the LCEN. When the ratio of storage and loss modulus is considered as shown in Figure 2c,d, the initial magnitudes of a precure time "t_1" can be compared to a postcure time "t_2". As observed in Figure 2a,b, the magnitudes of the neat and modified materials are similar in both low- and high-shear test conditions, suggesting that the effects of the fumed silica on the cure on the time-dependent rheological properties are minimal.

Figure 2 demonstrates that the additive introduced provides minimal effect on the time-dependent rheological properties and the cure profile; therefore, other properties must also be considered when using rheology as a predictor of 3D printability. Namely, the degree of shear-thinning and yield strength are of particular consideration. High degrees of shear thinning may be preferable for 3D printing such that a bead of epoxy ink or LCEN may be readily extruded and formed under high-shear environments. Furthermore, the ink or LCEN should show increased viscosity under the effects of low-shear such as in the condition of maintaining the deposited bead shape and supporting the deposition of additional beads in the positive-z build direction. High viscosity under low-shear alone is not sufficient as some flow may still be observed over the cure times associated with the latent heat cure of the LCEN.

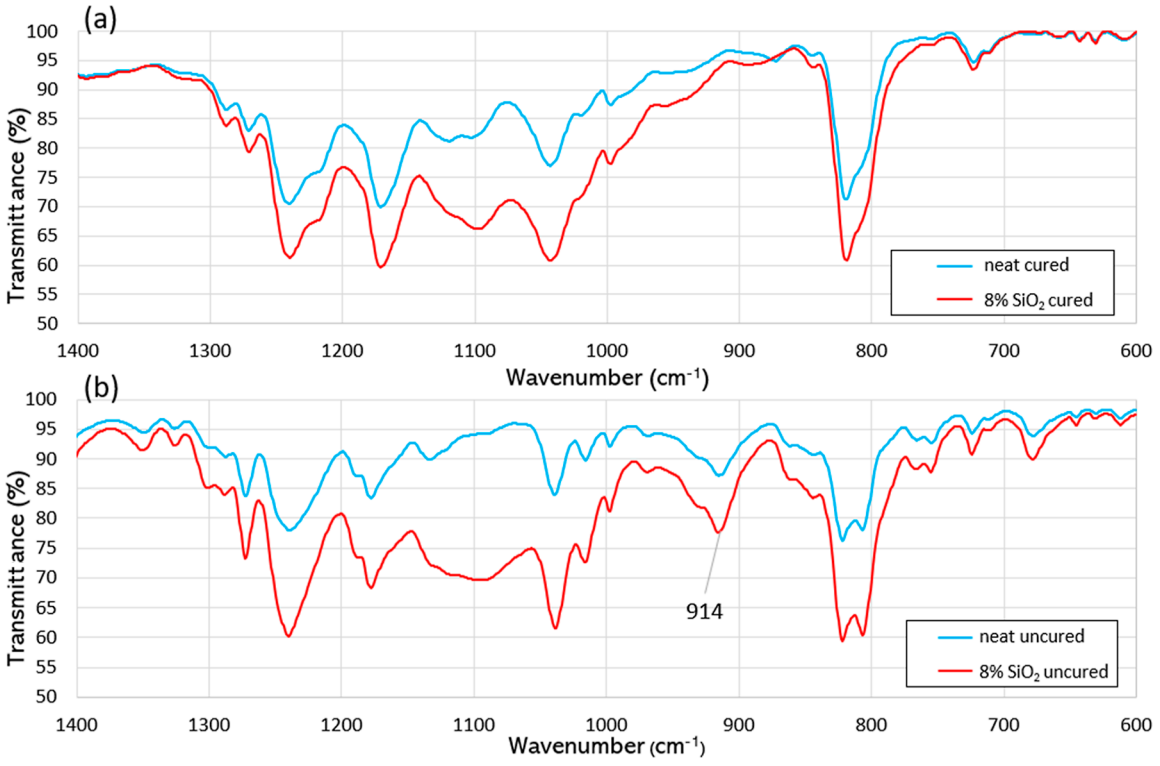

Figure 8. FTIR of neat and modified cured LCEN (a) and uncured systems (b). A broad characteristic peak between 1300 and 1000 cm^{-1} is noted for SiO_2.

https://doi.org/10.1021/acsomega.4c05664
ACS Omega 2024, 9, 40801−40809

For this reason, yield stress must also be considered. With a sufficiently high yield stress, flow can be inhibited such that the integrity of a deposited bead is maintained even under latent heat cure time and temperature. Yield stress of a viscoelastic LCEN is determined by a flow test, as described in Figure 3.

From the photography in Figure 3, complex viscosity in excess of 1×10^5 Pa s alone is not sufficient to prevent material flow at the cure temperature, as seen in the neat LCEN. The fumed silica additive is observed to increase the yield stress of the uncured LCEN over 4 orders of magnitude, from 0.096 to 184 Pa with an 8% wt addition of the fumed silica. Furthermore, the shear rate-dependence of viscosity of the LCEN can be measured with the flow test. Once the yield stress of the uncured neat LCEN has been exceeded, the viscosity is observed to undergo little change with the increasing shear rate, suggesting very weak shear thinning properties. For the modified uncured LCEN, a continuous reduction in viscosity is observed with the increase of shear rate, indicating a much stronger shear thinning behavior. From these measurements, a yield stress of at least ∼180 Pa at the print and cure temperature is recommended as an additional predictive property of 3D printability in a viscoelastic fluid.

The magnitude of the enthalpy of the LC isotropic transformation temperature is directly related to the degree of liquid crystallinity of the LCEN.[12] The DSC measurements, as shown in Figure 4, demonstrate a reduction in enthalpy from neat and modified LCEN, suggesting that the fumed silica additive hinders the formation of LC domains. Shape memory is discussed as being facilitated by the alignment of different liquid crystal domains; therefore, when fewer domains are available, less recoverable strain is achieved by thermal cycling. This might also be seen in Figure 5, where the achievable strain under static load thermal cycling of the modified LCEN is much lower than that of the neat LCEN.

The 3D printed shape of the modified LCEN successfully retained its shape during the cure process, allowing it to be evaluated for shape memory, as shown in Figure 5a. The printed shape was deformed at 100 °C and allowed to cool to room temperature in the deformed state. From room temperature, the deformed print was allowed to recover after heating above the phase transformation temperature. The print was observed to recover to its original conformation within 5 min. Furthermore, cast samples of neat LCEN and the modified LCEN samples were subjected to a constant tensile load of 0.1 MPa while the temperature was incrementally increased and decreased between 80 and 140 °C for multiple cycles at a constant rate of 1 °C/min, with a 1 min dwell time at each extreme. The neat LCEN achieved recoverable strain in excess of 100% while the modified only reached 14% strain under the static loading conditions. During the first heat cycle under loading, the LCEN experiences two sequential effects. First, the material becomes sufficiently ductile, and the network becomes sufficiently mobile for the strain-induced alignment of LC domains with respect to the loading direction to occur, resulting in a large initial strain. This is the P−M transformation described earlier in the work. Soon after, the temperature is increased beyond the isotropic transformation temperature T_i, causing all alignment within the LC domain to be lost. Because the large initial strain of the P−M transformation was owed to the alignment of LC domains, the strain is reduced in their absence above T_i. In the case of both the neat and the silica-modified LCEN, dimensional stability of the shape memory behavior was observed, with consistently toggleable fixed high-strain and fixed low-strain states across T_i. This is seen in the closed hysteresis loop behavior of the shape memory effects in Figure 5b.

WAXS measurements were performed to verify the formation of LC domains. Furthermore, the intensity variation in the azimuthal direction under strain indicates a change in the alignment of the domains. The measurements reveal that a positional ordering exists within the LCEN, that is, the observed rings in the undeformed state have a constant azimuthal intensity. This indicates the presence of LC domains that are allowed to randomly orient in the flexible amorphous domains in the LCEN. In Figure 6, under the deformed condition, the azimuthal intensity is observed to transition to two well-defined peaks under similar q-spacing to the undeformed case. All samples exhibited similar q-spacing, which is demonstrated in Supporting Information in Figure S1. In this case, the spacing in the LC domains is minimally affected by the deformations; however, the domains themselves are allowed to rotate and align in the flexible amorphous region. In this way, the spacing of mesogens does not change, but a greater number of mesogens are aligned in the network of the LCEN. In Figure 6b, a similar behavior in the fumed silica-modified LCEN is observed; however, a much lessened alignment effect is noted. The peaks in the deformed state are found to have a much smaller intensity than the deformed intensities in the neat counterpart of Figure 6a. This suggests that the degree of alignment for an applied strain is inhibited by the presence of the fumed silica, though the deformation and alignment that is afforded are still recoverable across a single thermal cycle through the phase transformation temperature.

By viewing the LCEN under a columnar polarized lens, such as in Figure 7, the presence of LC domains is evident by the variation in transmitted light as the filter orientation rotates and changes from aligned and misaligned mesogenic orientation within domains. Within the neat LCEN, a greater area fraction of regions of variable light transmittance is shown compared to the modified LCEN, suggesting a higher degree of liquid crystallinity and higher degree of LC domain formation in the neat LCEN, a claim that has been further corroborated by DSC.

General observations of the FTIR spectra shown in Figure 8 are that there is little meaningful difference between neat and modified, strengthening the argument that the additive does not affect cure or chemistry, but it does affect morphology, shown in increased yield shear stress, decreased participation of LC domains in P−M transformation, and decreased formation of LC domains. Furthermore, the lack of new bond types in FTIR suggests that the interaction between the matrix and fumed silica is mostly physical with little to no chemical bonding between it and the epoxy matrix. The physical interactions of the silica and the matrix are more directly observed in shape memory testing, azimuthal intensity spectra from WAXS, reduced isotropic transformation energy from DSC, and polarized light microscopy, each of which indicates a reduction in the liquid crystal volume fraction and a hindrance in the LC domains to participate in the P−M transformation that facilitates shape memory. Of note also is the disappearance of the 914 cm^{-1} peak characteristic of epoxide after curing, indicating that a complete cure was achieved. Additionally, the separation in the transmittance spectra between neat and silica modified is due to a broad peak characteristic of fumed silica between 1300 and 1000 cm^{-1}.

https://doi.org/10.1021/acsomega.4c05664
ACS Omega 2024, 9, 40801−40809

Full FTIR spectra of all base components, including fumed silica, are available in the Supporting Information in Figure S2.

4. CONCLUSIONS

A two-component LCEN was evaluated for 3D printing by tuning the rheology by using fumed silica. It was found that printing such an LCEN with a latent heat cure can be achieved by ensuring that a minimum yield shear stress is achieved at the cure temperature of the LCEN. Furthermore, it was found that the presence of fumed silica has multiple effects on the LCEN morphology, as suggested by changes in enthalpy in DSC and reduction in visible area fraction of domains under polarized light microscopy. First, the fumed silica increased the zero-shear viscosity and yield stress such that printability could be achieved while also producing an uncured mixture of sufficient integrity that the printed shape is preserved during the cure. The presence of fumed silica also reduces the degree of liquid crystallinity from that of a neat LCEN under similar curing conditions. Furthermore, the fumed silica partially inhibits the ability of the LC domains in the LCEN to participate in the P−M transformation under axial tensile loading. Despite the changes in morphology and partial inhibition of formation of LC domains, shape memory is demonstrated to maintain a capability, albeit with reduction is achievable strain during the P−M transformation. This demonstration enables future investigation of the relationship of LC domain formation and functional capabilities and the use of morphological modification as a means for tuning functional capabilities of LCEN.

■ ASSOCIATED CONTENT

Supporting Information

The Supporting Information is available free of charge at https://pubs.acs.org/doi/10.1021/acsomega.4c05664.

Integration of azimuthal intensity of 2D WAXS spectra for each LCEN sample and full FTIR spectra of the individual unmixed components used in all LCEN samples (PDF)

■ AUTHOR INFORMATION

Corresponding Author

David P. Harper − *Center for Renewable Carbon, University of Tennessee, Knoxville, Tennessee 37996-4570, United States;* orcid.org/0000-0003-2783-5406; Email: dharper4@utk.edu

Authors

Collin Pekol − *Department of Materials Science and Engineering, The University of Tennessee, Knoxville, Tennessee 37996-4519, United States;* orcid.org/0000-0002-9193-7426

Jacob Furst − *Department of Materials Science and Engineering, The University of Tennessee, Knoxville, Tennessee 37996-4519, United States*

Yuzhan Li − *School of Materials Science and Engineering, University of Science and Technology, Beijing 100083, China;* orcid.org/0000-0002-7432-2251

Jong Keum − *Spallation Neutron Source, Oak Ridge National Laboratory, Oak Ridge, Tennessee 37830, United States*

Complete contact information is available at: https://pubs.acs.org/10.1021/acsomega.4c05664

Notes

The authors declare no competing financial interest.

■ ACKNOWLEDGMENTS

SAXS, MAXS, and WAXS measurements were enabled by the Major Research Instrumentation program of the National Science Foundation under award no. DMR-1827474. This work was also enabled by the Center for Materials Processing (CMP) by means of providing chemicals and instrumentation.

■ REFERENCES

(1) Rios, O.; Carter, W.; Post, B.; Lloyd, P.; Fenn, D.; Kutchko, C.; Rock, R.; Olson, K.; Compton, B. 3D printing via ambient reactive extrusion. *Mater. Today Commun.* **2018**, *15* (C), 333−336.

(2) Sudbury, T. Z.; Springfield, R.; Kunc, V.; Duty, C. An assessment of additive manufactured molds for hand-laid fiber reinforced composites. *Int. J. Adv. Manuf. Technol.* **2017**, *90* (5−8), 1659−1664.

(3) Compton, B. G.; Lewis, J. A. 3D-Printing of Lightweight Cellular Composites. *Adv. Mater.* **2014**, *26* (34), 5930−5935.

(4) Sutton, J. T.; Rajan, K.; Harper, D. P.; Chmely, S. C. Lignin-Containing Photoactive Resins for 3D Printing by Stereolithography. *ACS Appl. Mater. Interfaces* **2018**, *10* (42), 36456−36463.

(5) Zhang, Z.; Corrigan, N.; Boyer, C. A Photoinduced Dual-Wavelength Approach for 3D Printing and Self-Healing of Thermosetting Materials. *Angew. Chem., Int. Ed.* **2022**, *61* (11), No. e202114111.

(6) Jin, F.-L.; Li, X.; Park, S.-J. Synthesis and application of epoxy resins: A review. *J. Ind. Eng. Chem.* **2015**, *29*, 1−11.

(7) Li, Y.; Liu, T.; Ambrogi, V.; Rios, O.; Xia, M.; He, W.; Yang, Z. Liquid Crystalline Elastomers Based on Click Chemistry. *ACS Appl. Mater. Interfaces* **2022**, *14* (13), 14842−14858.

(8) Pang, X.; Lv, J.; Zhu, C.; Qin, L.; Yu, Y. Photodeformable Azobenzene-Containing Liquid Crystal Polymers and Soft Actuators. *Adv. Mater.* **2019**, *31* (52), No. e1904224.

(9) Ware, T. H.; McConney, M. E.; Wie, J. J.; Tondiglia, V. P.; White, T. J. Voxelated liquid crystal elastomers. *Am. Assoc. Adv. Sci.* **2015**, *347* (6225), 982−984.

(10) Romberg, S. K.; Islam, M. A.; Hershey, C. J.; DeVinney, M.; Duty, C. E.; Kunc, V.; Compton, B. G. Linking thermoset ink rheology to the stability of 3D-printed structures. *Addit. Manuf.* **2021**, *37*, 101621.

(11) Zhang, Q.; Wu, C.; Song, Y.; Zheng, Q. Rheology of fumed silica/polypropylene glycol dispersions. *Polymer* **2018**, *148*, 400−406.

(12) Li, Y.; Pruitt, C.; Rios, O.; Wei, L.; Rock, M.; Keum, J. K.; McDonald, A. G.; Kessler, M. R. Controlled Shape Memory Behavior of a Smectic Main-Chain Liquid Crystalline Elastomer. *Macromolecules* **2015**, *48* (9), 2864−2874.

(13) Haskew, M. J.; Hardy, J. G. A Mini-Review of Shape-Memory Polymer-Based Materials. *Johnson Matthey Technol. Rev.* **2020**, *64*, 425−442.

(14) Mohr, R.; Kratz, K.; Weigel, T.; Lucka-Gabor, M.; Moneke, M.; Lendlein, A. Initiation of Shape-Memory Effect by Inductive Heating of Magnetic Nanoparticles in Thermoplastic Polymers. *Proc. Natl. Acad. Sci.* **2006**, *103* (10), 3540−3545.

(15) Albini, A. Some remarks on the first law of photochemistry. *Photochem. Photobiol. Sci.* **2016**, *15* (3), 319−324.

(16) Lendlein, A.; Langer, R. Biodegradable, Elastic Shape-Memory Polymers for Potential Biomedical Applications. *Science* **2002**, *296* (5573), 1673−1676.

(17) Pei, Z.; Yang, Y.; Chen, Q.; Terentjev, E. M.; Wei, Y.; Ji, Y. Mouldable liquid-crystalline elastomer actuators with exchangeable covalent bonds. *Nat. Mater.* **2014**, *13* (1), 36−41.

(18) Li, Y.; Ambrogi, V.; Cerruti, P.; Goswami, M.; Yang, Z.; Kessler, M. R.; Rios, O. Functional liquid crystalline epoxy networks and composites: from materials design to applications. *Int. Mater. Rev.* **2022**, *67* (2), 201−229.

(19) Li, Y.; Goswami, M.; Zhang, Y.; Liu, T.; Zhang, J.; Kessler, M. R.; Wang, L.; Rios, O. Combined light- and heat-induced shape

memory behavior of anthracene-based epoxy elastomers. *Sci. Rep.* **2020**, *10* (1), 20214.
(20) Li, Y.; Keum, J. K.; Wang, J.; Jiang, N.; Bras, W.; Kessler, M. R.; Rios, O. Multiscale Structural Characterization of a Smectic Liquid Crystalline Elastomer upon Mechanical Deformation Using Neutron Scattering. *Macromolecules* **2021**, *54* (22), 10574−10582.
(21) Li, Y.; Rios, O.; Keum, J. K.; Chen, J.; Kessler, M. R. Photoresponsive Liquid Crystalline Epoxy Networks with Shape Memory Behavior and Dynamic Ester Bonds. *ACS Appl. Mater. Interfaces* **2016**, *8* (24), 15750−15757.
(22) Lee, J. Y.; Jang, J.; Hwang, S. S.; Hong, S. M.; Kim, K. U. Synthesis and curing of liquid crystalline epoxy resins based on 4,4′-biphenol. *Polymer* **1998**, *39* (24), 6121−6126.

https://doi.org/10.1021/acsomega.4c05664
ACS Omega 2024, 9, 40801−40809